JISSE
ISSN: 2636-4425

Journal of International Society for Science and Engineering
Vol. 3, No. 1, 13-17 (2021)

JISSE
E-ISSN:2682-3438

Numerical Investigation of The Effect of Airfoil Trailing Edge Inflation at low Reynolds Number

Ayman I. Bakry[1], Mohamed K.K. Khalil[2],
Ali M. Elzahaby[1], Amr A. El-Feky[3], Ahmed S. Mohamed[1]

[1]Department of Mechanical Power, Tanta University, Egypt.
[2]Department of A/C Mechanics, Military Technical College, Egypt.
[3]Department of Mechanical Engineer, National Research Center, Egypt

ARTICLE INFO

Article history:
Received:2020-08-26
Accepted:2021-03-01
Online: 2021-03-01

Keywords:
NACA0021
Trailing edge inflation
Passive Stall Control

ABSTRACT

To investigate the effect of airfoil shape design on aerodynamics of the airfoil, a new modified airfoil shape design is introduced in this paper. Thick symmetrical NACA 0021 airfoil is used as base model in this study that the trailing edge end curvature was altered in design shape to be inflated to have 25%, 50% and 100% scaled of the leading-edge curvature at the same cord length and same maximum thickness data. Numerical investigation, using shear-stress transport kω-SST turbulence model, is performed to study the effect of airfoil trailing edge inflation on the aerodynamic characteristics at low Reynolds Number. The base airfoil model, NACA0021, is validated numerically and shows a good agreement with previous experimental results. The results show that the new modified airfoil with 100% inflation delays the flow separation to higher angle of attack and increases the maximum lift coefficient about 40% compared with the base NACA0021 airfoil.

1. Introduction

The pre-historical roots of flow control art probably belong to the invention of streamlined spears, boomerangs, and feathers fin stabilized arrows.[1] The development of this art has been extending through five years: the empirical era, prior to 1900, the scientific era 1900-1940, the World War II era 1940-1970, the energy crisis era 1970-1990, and the 1990s and beyond. There are different methods to control the stall. Some types required external actuation which called the active stall control. The other types are called passive stall control don't require any actuation in the rotor blade. The Passive control mean using the energy in the oncoming flow and doesn't depend on external actuation. Methods that most used as a passive stall control by using vortex generators [2 - 19] for decreasing the flow separation by generation of a series of vortices over the upper surface of the airfoil. These vortices guide the high momentum fluid in the free stream to the near the airfoil wall. This high energy supplies the boundary layers with additional momentum, which allows them to penetrate further against adverse pressure gradients before separating. Also, leading-edge sinusoidal protuberances inspired from the Hampack whale fines causes to increases the generated lift up to 50% greater than the baseline foil with no increasing drag. [20, 21]. Adding a circular cavity is considered to be passive stall control [22 - 24], it behaves as a reverse flow reservoir. In general, the oscillations of the shear layer above the cavity generate small vortices, which causes a delay in separation of the boundary layer in cavity downstream and generates additional lift force. Turbulence promoter [25 - 27] like protuberance, improve the aerodynamic performances without additional drag by tripping wire near the leading edge. The promoter the lift coefficients at high angle of attack. Another type of passive stall control is using micro-cylinder. It also provides enhancement of lift-to-drag ratio after stall with decreasing in drag coefficient. [28] Changing in airfoil profile is considered also to be a type of stall control like Step Airfoil (airfoils with Kline Fogelman variants), similar to the airfoil cavity, it works as a vortex trap but not only the Kline-Fogelman [29 - 31] airfoils resists stalling for very high angles but also prevents the free fall usually observed at critical angles. Lower surface stepped airfoil also shows increasing in coefficient of lift (Cl) and increasing in lift to drag ratio (L/D) over conventional airfoil values [32] Change the design of the

* Ahmed S. Mohamed, Department of Mechanical Power, Tanta University, Tanta, Egypt, +201159775550, ahmedderbaz@yahoo.com

trailing edge shape that affect the aerodynamic forces on the airfoil is our concerned in this study. The trailing edge curvature end was assumed to be altered in design shape to be inflated to have 25%, 50% and 100% scaled of the leading-edge curvature at low Reynolds Number with preserving cord length and maximum thickness of the base airfoil 0021.

2. Numerical Discretization:

It is required, as it well known, three steps for carrying out the numerical simulation. First step is creating models and surrounding domains. Constructing the mesh is the second step required for the simulation. It is done by using Pointwise commercial software. The final step is using ANSYS FLUENT 16.5 commercial software package as a solver based on cell-centered finite volume approach to solve the Navier-Stokes equations which consists of Partial Differential Equations (PDEs) describing the laws of conservation for continuity, momentum, and energy equations. Calculations are done by Workstation with 24 cores and 48 Giga Rams.

2.1. Computational Domain and Boundary Condition

The base airfoil used in the simulation is the symmetrical airfoil NACA0021 with cord length 0.14 m. The modification is introduced into trailing edge, that the trailing edge end curvature was altered in design shape to be inflated to have 25%, 50% and 100% scaled of the leading-edge curvature at the same cord length as seen in Fig.1 at different angles of attack to determine a wide range of airfoil characteristics for all models within this study. Fig.2 represents the variation of the airfoil trailing edge inflation percentage to base airfoil area ratios which yields an increasing with increase the trailing edge inflation percentage.

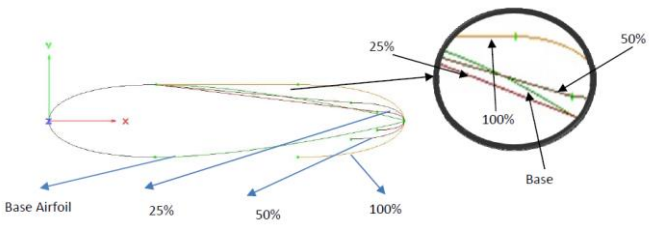

Fig. 1 Symmetrical Airfoil 0021 with 25%, 50% and 100% trailing edge inflations of scaled of the leading-edge curvature.

The outer domain is constructed as a C domain as shown in Fig.3. The outer domain is extended 10 times the chord length in the upstream and 20 times in the downstream. The height of domain is designed to be 20 times chord length. Inlet and outlet of the domain are defined as the velocity inlet and pressure outlet respectively. Upper and downside of domains are set to be symmetric boundary condition.

2.2. Grid System

Structured grids are used to discretize the computational domain of 1,477,507 total cells as seen in Fig.4. a., b and c. Grid points are clustered around the airfoils leading and trailing edges as shown in Fig. 4.b and c respectively with 1100 grid points on its surface to preserve the y+ near the airfoil wall less than 1.

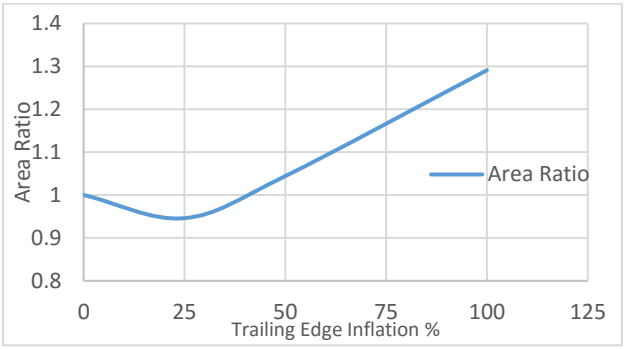

Fig.2 Variation of the airfoil trailing edge inflation percentage to base airfoil area ratios

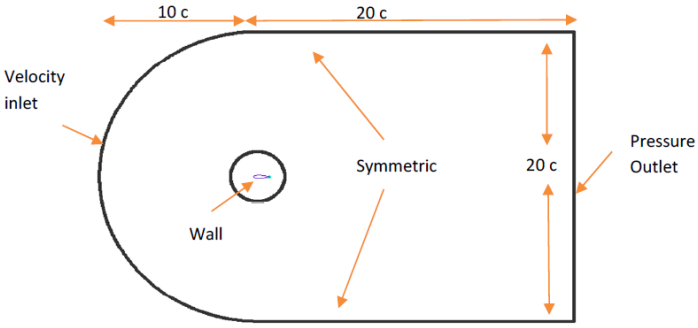

Fig. 3 Computational Domain and Boundary Conditions, Wall = Airfoil

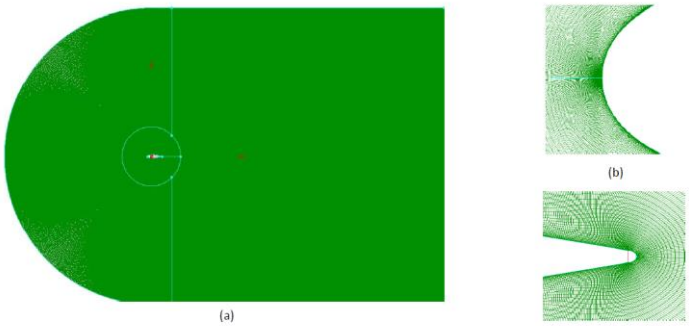

Fig. 4 Grid System of (a) Entire domain. (b) Leading Edge mesh. (c) Trailing Edge mesh

2.3. Turbulence Model

The shear-stress transport kω-SST model, developed by Menter [33], is used in the simulation. The turbulence kinetic energy k and the specific dissipation rate ω, are obtained from the following transport equations

$$\frac{\partial}{\partial t}(\rho k) + \frac{\partial}{\partial x_j}\left(\rho k \underline{u_j}\right) = \frac{\partial}{\partial x_j}\left[\Gamma_k + \frac{\partial k}{\partial x_j}\right] + G_k - Y_k + S_k \quad (1)$$

$$\frac{\partial}{\partial t}(\rho \omega) + \frac{\partial}{\partial x_i}(\rho \omega u_i) = \frac{\partial}{\partial x_j}\left[\left(\Gamma_\omega + \frac{\partial \omega}{\partial x_j}\right)\right] + G_\omega + Y_\omega + S_\omega \quad (2)$$

Where G_k is generation of turbulence kinetic energy due to mean velocity gradients. G_ω represents the generation of ω. Γ_k and Γ_ω represent the effective diffusivity of k and ω respectively. Yk and Yω represent the dissipation of k and ω, respectively, due to turbulence. Sk and Sω are user-defined source terms. The effective diffusivities for the model can be calculated form equations (3) and (4) [33].

$$\Gamma_k = \mu + \frac{\mu_t}{\sigma_k} \quad (3)$$

$$\Gamma_\omega = \mu + \frac{\mu_t}{\sigma_\omega} \quad (4)$$

$$\mu_t = \alpha^* \frac{\rho k}{\omega} \quad (5)$$

$$\alpha^* = \alpha^*_{inf}\left(\frac{0.024+\frac{Re_t}{6}}{1+\frac{Re_t}{6}}\right) \quad (6)$$

$$Re_t = \frac{\rho k}{\mu \omega} \quad (7)$$

That σ_k and σ_ω are the turbulent Prandtl numbers for k and ω, α^* is coefficient damps the turbulent viscosity causing a low-Reynolds number correction.

The investigation is done under unsteady conditions with time step 0.001. Coupled algorithm is chosen to solve the momentum and pressure-based continuity equations together. The discretization schemes for the pressure equation are second order and for Momentum, Turbulent kinetic energy, and specific dissipation rate is second order upwind.

3. Case Study

To validate the CFD model with experiments, the numerical results was validated with experimental results published by Holst et al. [34]. The experiments presented were conducted in closed loop laminar wind tunnel with turbulence level less than 0.5 %. NACA0021 airfoil profile used within the present study is mounted between two splitter plates to ensure a 2D flow around the profile section and has a chord 0.14 m, a span 0.28 m, and thus an aspect ratio 2 at Reynolds number .1.8 x 10^5. The airfoil mounting allows full angle of attacks 360 degrees angle variations. By comparing the lift and drag coefficients as shown in Fig 5. a and b, it is found that results show good agreement with the experimental data.

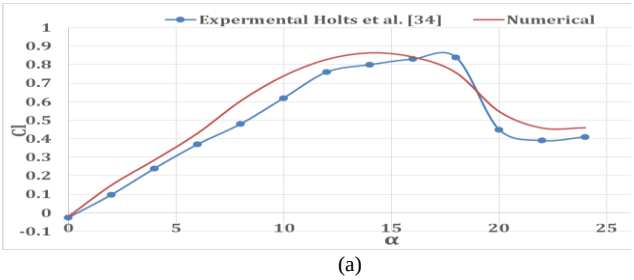

(a)

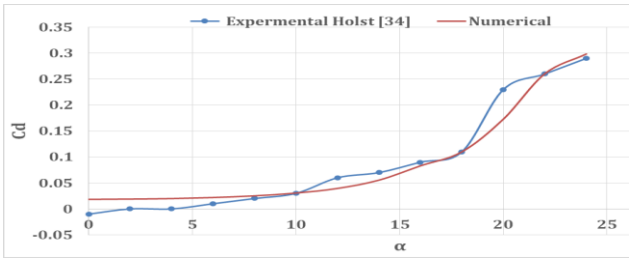

(b)

Fig. 5 Model Validation with the experimental [34] of (a) Lift Coefficient (b) Drag Coefficient.

4. Results and discussions:

Numerical results introduce the onset of flow separation of the base NACA 0021 airfoil at angle of attack 14º as shown in Fig. 6.a_1 while the rest of the flow over the airfoil upper surface remains attached. The flow separation increases at much higher angle of attack moving from trailing edge to leading edge and two attached vortices with opposite rotation developed at airfoils downstream as seen in Fig. 6.b_1 and Fig.6.c_1 which represent the flow separation at angles 16º and 18º respectively. The two vortices downstream the airfoil moved upwards causing the upper vortex to be larger than lower vortex at angle 22º as seen in Fig.6.d_1. By its turn causes the reduction in the produced lift coefficient and increasing in drag coefficient as seen in Fig.7.and b. In case of 25% trailing edge inflations, the slope of its straight upper surface is much higher than in case of the base airfoil, which causes an early flow separation compared to the base airfoil as shown in Fig. 4.a_2, but decreasing in its surface area, as seen in Fig.2, causes to increase the generated maximum lift coefficient nearly 20% at 10º angle of attack as seen in Fig. 7.a. The flow separation occurs at higher angle of attacks and increases rapidly which causes to dramatically decrease the lift coefficient and increases the drag coefficient as shown in Fig.7.and b. respectively. By increasing the inflation percentage to be 50%, decreases the straight upper surface slope compared with previous case but the flow separation occurs earlier than the base airfoil case as seen in Fig.6.a_1, which accuses to delay the flow separation to angle of attack 12º at which the maximum lift coefficient increases 36% compared to the base airfoil due to the increasing in surface area. In case of 100% inflation, it causes to delay the separation to angle of attack 18º as seen in Fig. 4.c_4 and the maximum lift coefficient increase by 45% compared to the base airfoil due to increasing in the surface area and decreasing in the straight upper surface slope. As angle of attack was increased, flow velocity increased near the leading edge on the suction surface, causing a sharp decrease of the pressure coefficient distribution for all models as seen in Fig.8. The pressure coefficient profiles on the suction surface were found to rapidly reach their negative peaks near the leading edge and thereafter recover gradually on the downstream portion of the airfoil models. Also, the flow velocity magnitude increases over the downstream half of the pressure side causing a decrease of pressure.

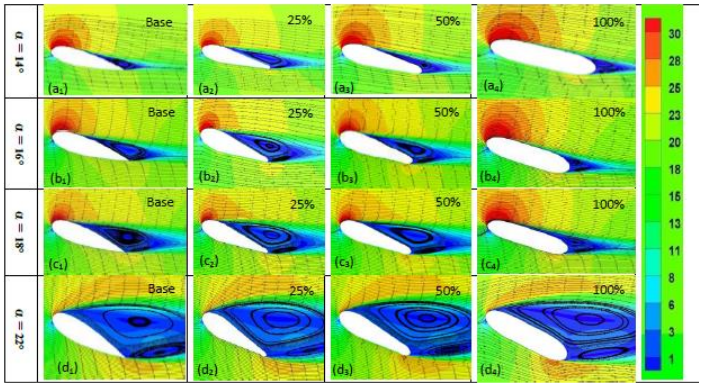

Fig.6 Velocity magnitude and stream lines of base NACA 0021 airfoil, 25%, 50% and 100% trailing edge inflations of scaled of the leading edge curvature at different angles of attack at Re = 180k

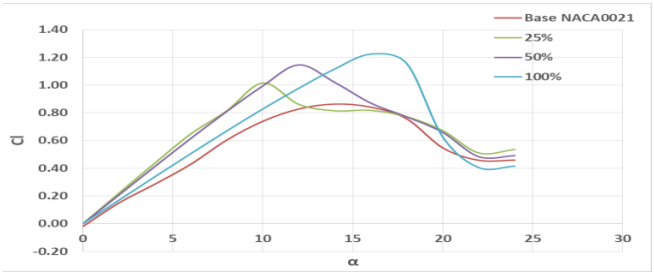

(a)

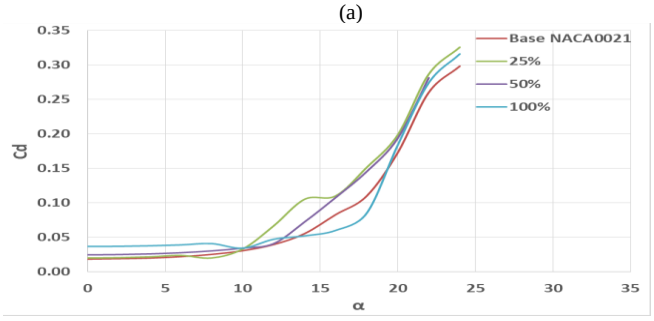

(b)

Fig 7: Lift (a) and drag (b) coefficients comparisons for the three modified airfoils compared with the base airfoil.

At angle 14º, increasing the trailing edge inflation to 25% causes to increase PDE acting on the upper surface due to the larger slope of the straight upper surface compared to the base airfoil as mentioned before in Fig.1. At much higher inflation angle, more than 25%, the increasing in the trailing edge inflation causes to decreases the pressure coefficient acting on the upper surface. At 16º and 18º angles of attack, shown in Fig.8, b and c indicates that the 100% trailing edge inflation generate lower Cp over the upper surface and shows a good stall characteristic compared to the other cases. At angle 22º angle of attack, a fully stall occurs to the all airfoils, which causes to increase the pressure coefficient acting on the airfoils upper surface, and by turn decreases the generated lift coefficient at this angle of attack as shown in Fig.7.a. Due to the similar leading edge shape of the trailing edge at 100% trailing edge inflation, the velocity magnitude increases as at the trailing edge lower surface, as seen in Fig.6.d which causes by turn decreases the pressure coefficient acting on the lower surface.

5. Conclusions

A two-dimensional incompressible unsteady flow investigation is performed for NACA 0021 with modified trailing edge that have 25%, 50% and 100% scaled of the leading-edge curvature at the same cord length. It is concluded that the 100% inflation shows good stall characteristics and delays the flow separation to higher angle of attack and increases the maximum lift coefficient about 40% compared to the base airfoil.

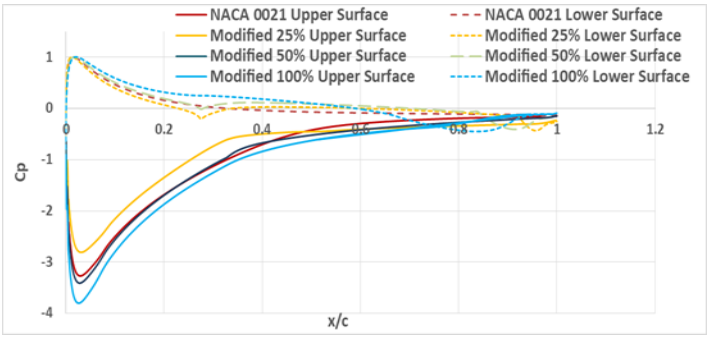

(a)

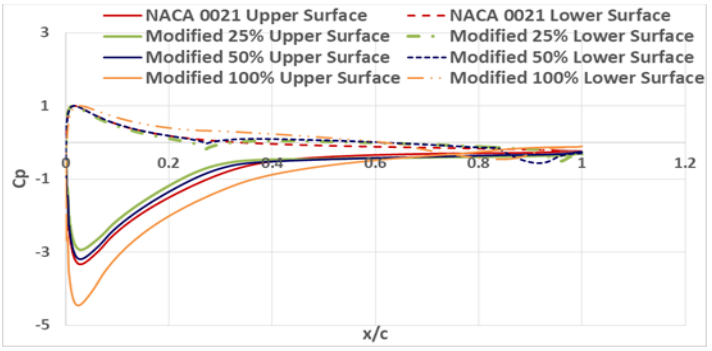

(b)

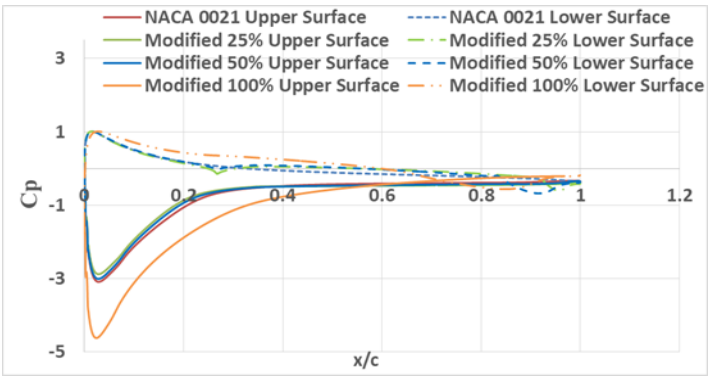

(c)

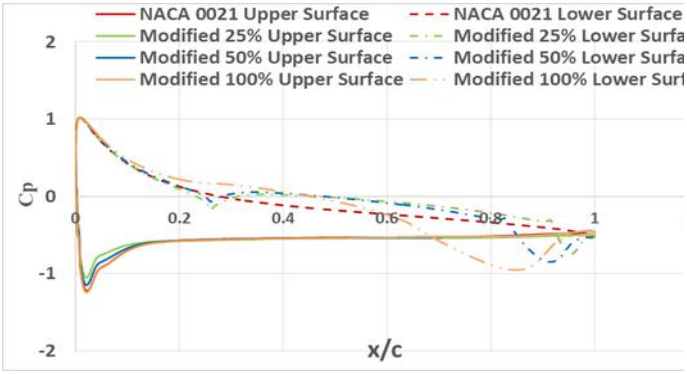

(d)

Fig. 8 Variation of pressure coefficient acting on the airfoil upper surface and lower surface of base, 25%, 50% and 100% trailing edge inflation percentage at angles of attack (a)14^o (b)16^o (c)18^o (d) 22^o.

6. Reference

[1] M. Gad-el-Hak, "Modern Developments in Flow Control," Appl. Mech. Rev., vol. 49, no. 7, p. 365,1996.

[2] S. Shun and N. A. Ahmed, "Wind turbine performance improvements using active flow control techniques," Procedia Eng., vol. 49, no. mm, pp. 83–91, 2012.

[3] S. A. Prince, V. Khodagolian, C. Singh, and T. Kokkalis, "Aerodynamic Stall Suppression on Aerofoil Sections Using Passive Air-Jet Vortex Generators," AIAA J., vol. 47, no.9, pp. 2232–2242, 2009.

[4] G. V. Selby, J. C. Lin, and F. G. Howard, "Control of low-speed turbulent separated flow using jet vortex generators," Exp. Fluids, vol. 12, no. 6, pp. 394–400, 1992.

[5] A. Krzysiak, "Control of Flow Separation Using Self-Supplying Air-Jet Vortex Generators," AIAA J., vol. 46, no. 9, pp. 2229–2234, 2008.

[6] J. P. Johnston, "Vortex Generator Jets—Means for Flow Separation Control," AIAA J., vol. 28, no. 6, pp. 989–994, 1990.

[7] S. A. Prince, C. Badalamenti, and C. Regas, "The application of passive air jet vortex-generators to stall suppression on wind turbine blades," Wind Energy, vol. 20, no. 1, pp. 109–123, 2017.

[8] A. R. Paul, "" Slotted flow separation control over a NACA2412 airfoil " SLOTTED FLOW SEPARATION CONTROL OVER A NACA 2412 AIRFOIL," no. December 2012, 2015.

[9] S. a. Prince, V. Khodagolian, C. Singh, and T. Kokkalis, "Aerodynamic Stall Suppression on Aerofoil Sections Using Passive Air-Jet Vortex Generators," AIAA J., vol. 47, no. 9, pp. 2232–2242, 2009.

[10] H. Mai et al., "Dynamic Stall Control by Leading Edge Vortex Generators," J. Am. Helicopter Soc., vol. 53, no. 1, p. 26, 2008.

[11] A. Choudhry, M. Arjomandi, and R. Kelso, "Methods to control dynamic stall for wind turbine applications," Renew. Energy, vol. 86, pp. 26–37, 2016.

[12] C. M. Velte, M. O. L. Hansen, and D. Cavar, "Flow analysis of vortex generators on wing sections by stereoscopic particle image velocimetry measurements," Environ. Res. Lett., vol. 3, no.1, 2008.

[13] N. Souckova, D. Simurda, and L. Popelka, "Control of Boundary Layer Separation on Flapped Airfoil with Low-Profile Vortex Generator," Exp. Fluid Mech. 2009, Proc. Int. Conf., pp.310–315, 2009.

[14] J. C. Lin, Review of research on low-profile vortex generators to control boundary-layer separation, vol. 38, no. 4–5. 2002.

[15] M. S. Chandrasekhara, "Optimum Gurney flap height determination for 'lost lift' recovery in compressible dynamic stall control," Aerosp. Sci. Technol., vol. 14, no. 8, pp. 551–556, 2010.

[16] W. T. Study, "Water Tunnel Study of," Water, no. November 1988.

[17] M. P. Kinzel, M. D. Maughmer, and E. P. N. Duque, "Numerical Investigation on the Aerodynamics of Oscillating Airfoils with Deployable Gurney Flaps," Aiaa J., vol. 48, no. 7, pp. 1457–1469, 2010.

[18] D. Jeffrey, X. Zhang, and D. W. Hurst, "Aerodynamics of Gurney Flaps on a Single-Element High Lift Wing," J. Aircr., vol. 37, no. 2, pp. 295–301, 2000.

[19] D. T. Y. Nakafuji, C. P. van Dam, R. L. Smith, and S. D. Collins, "Active Load Control for Airfoils using Microtabs," J. Sol. Energy Eng., vol. 123, no. 4, p. 282, 2001.

[20] A. Gawad, "Numerical Simulation of the Effect of Leading-Edge Tubercles on the Flow Characteristics Around an Airfoil," Proc. ASME 2012 Int. Mech. Eng. Congr. Expo., pp. 1–9, 2012.

[21] H. Johari, C. W. Henoch, D. Custodio, and A. Levshin, "Effects of Leading-Edge Protuberances on Airfoil Performance," AIAA J., vol. 45, no. 11, pp. 2634–2642, 2007.

[22] D. Lasagna, R. Donelli, F. De Gregorio, and G. Iuso, "Effects of a trapped vortex cell on a thick wing airfoil," Exp. Fluids, vol. 51, no. 5, pp. 1369–1384, 2011.

[23] W. F. J. Olsman and T. Colonius, "Numerical Simulation of Flow over an Airfoil with a Cavity," AIAA J., vol. 49, no. 1, pp. 143–149, 2011.

[24] L. Zannetti, "Vortex equilibrium in flows past bluff bodies," J. Fluid Mech., vol. 562, pp. 151–171, 2006.

[25] F. Frunzulică, A. Dumitrache, and H. Dumitrescu, "Investigations of Passive Flow Control Devices for Vertical Axis Wind Turbines," Pamm, vol. 14, no. 1, pp. 723–724, 2014.

[26] K. Fukudome, M. Watanabe, A. Iida, and A. Mizuno, "Separation Control of High Angle of Attack Airfoil for Vertical Axis Wind Turbines," pp. 2–5.

[27] F. Frunzulica, A. Dumitrache, and B. Suatean, "Numerical investigations of passive flow control elements for vertical axis wind turbine," 10th Int. Conf. Math. Probl. Eng. Aerosp. Sci., vol. 331, pp. 331–340, 2014.

[28] D. Luo, D. Huang, and X. Sun, "Passive flow control of a stalled airfoil using a microcylinder," J. Wind Eng. Ind. Aerodyn., vol. 170, no. August, pp. 256–273, 2017.

[29] B. F. Mishriky and P. Walsh, "Effect of Step Depth and Angle in Kline-Fogleman (Kfm-2) Airfoil," vol. 16, no. 4, 2016.

[30] T. Nadu, "Study of Flow Field over Fabricated Airfoil Models of NACA 23015 with its Klinefogleman Variant," vol. 3, no. 2, pp. 95–100, 2013.

[31] F. Mishriky and P. Walsh, "Effect of the Backward-Facing Step Location on the Aerodynamics of a Morphing Wing," Aerospace, vol. 3, no. 4, p. 25, 2016.

[32] Md. Abdullah Bin Azizand Md. Shariful Islam "Effect of Lower Surface Modification on Aerodynamic Characteristics of an Airfoil" International Conference on Mechanical Engineering and Renewable Energy 2017, (ICMERE2017) 18 – 20 December 2017, Chittagong, Bangladesh

[33] "ANSYS Fluent Theory Guide," vol. 15317, no. November, pp. 724–746, 2013.

[34] d. Holst∗, "Experimental analysis of a NACA 0021 airfoil section through 180-degree angle of attack at low Reynolds numbers for use in wind turbine analysis," in turbomachinery technical conference and exposition, 2017, pp. 1–12.

7. Abbreviation and symbols

k	Turbulence kinetic Energy
ω	Specific Dissipation Rate
PDE	Partial Differential Equations
NACA	National Advisory Committee for Aeronautics
L	Lift force
D	Drag force
$\boldsymbol{G_k}$	generation of turbulence kinetic energy
$\boldsymbol{G_\omega}$	generation of ω
$\boldsymbol{\Gamma_k}$	effective diffusivity of
$\boldsymbol{\Gamma_\omega}$	effective diffusivity of ω
Yk	dissipation of k
Yω	dissipation of ω
Sk	turbulence.
Sω	turbulence
$\boldsymbol{\sigma_k}$	The turbulent Prandtl number of k
$\boldsymbol{\sigma_\omega}$	The turbulent Prandtl numbers for ω,
Cp	Coefficient of pressure
CL	Coefficient of lift
Cd	Coefficient of drag
C	Cord length of Airfoil